buildings

MDPI

Article

Parameter Study and Optimization of Static Performance for a Hybrid Cable-Stayed Suspension Bridge

Zhou Peng [1], Lijun Jia [1], Jiawei Xu [2], Kedian Luo [1] and Huiteng Pei [1,3,*]

[1] Department of Bridge Engineering, College of Civil Engineering, Tongji University, Shanghai 200092, China; tjpengzhou@tongji.edu.cn (Z.P.); jialj@tongji.edu.cn (L.J.); 2330982@tongji.edu.cn (K.L.)
[2] School of Civil and Environmental Engineering, Harbin Institute of Technology, Shenzhen 518055, China; jiaweixu@stu.hit.edu.cn
[3] Jiangxi Communication Design and Research Institute Co., Ltd., Nanchang 330052, China
* Correspondence: 2180098@tongji.edu.cn

Abstract: The hybrid cable-stayed and suspension (HCSS) bridge is known for its stability and cost-effectiveness, with significant application potential. This study examined the static performance of an HCSS bridge with a 1440 m main span. A finite element model (FEM) was developed to assess key parameters, such as the span-to-rise ratio, cable-to-hanger ratio, pylon stiffness, steel–concrete interface, and cable stiffness. Through FEM analysis and parameter optimization using the zero-order and first-order optimization methods in an ANSYS module, key design variables were optimized. The results show that an inappropriate span-to-rise ratio negatively impacts mid-span girder forces, while increasing the cable-stayed area enhances the overall stiffness. Main cable stiffness plays a crucial role in load-bearing and deformation control. Significant force differences were observed between stay and hanger cables, with axial force in the main girder increasing from the side span to the pylon under dead load. Bending moments in the transition region varied widely under combined loads. Optimizing parameters, such as the span-to-rise and cable-to-hanger ratios, significantly improved the mechanical performance of HCSS bridges, offering valuable insights for future designs.

Keywords: hybrid cable-stayed suspension bridge; mechanical performance; parameter study; parameter optimization

check for updates

Citation: Peng, Z.; Jia, L.; Xu, J.; Luo, K.; Pei, H. Parameter Study and Optimization of Static Performance for a Hybrid Cable-Stayed Suspension Bridge. *Buildings* **2024**, *14*, 3514. https://doi.org/10.3390/buildings14113514

Received: 29 September 2024
Revised: 21 October 2024
Accepted: 29 October 2024
Published: 3 November 2024

Copyright: © 2024 by the authors. Licensee MDPI, Basel, Switzerland. This article is an open access article distributed under the terms and conditions of the Creative Commons Attribution (CC BY) license (https://creativecommons.org/licenses/by/4.0/).

1. Introduction

Cable-supported bridges play a crucial role in bridge engineering, especially in medium- to long-span bridges, due to their exceptional structural performance, economic efficiency, and aesthetic appeal. This advantage stems from the innovative arrangement and interaction of its key components—the main cable system, the girder, and the pylons—with the main cable showing great flexibility, functioning as both a cable-stayed and suspension system, thus demonstrating high adaptability [1]. As design theory and construction techniques continue to advance, cable-stayed and suspension bridges exceeding a kilometer in span have become commonplace, transforming engineering marvels into the standard [2].

Recently, the booming global economy and increasing density of transportation networks have driven the demand for monumental bridges spanning vast seas. Major straits like the Strait of Gibraltar, the Tsugaru Strait, and the Bosphorus have become natural barriers to continental connectivity and exchange. Despite the success of traditional hybrid cable-stayed and suspension (HCSS) bridges, their limitations are becoming increasingly apparent with larger spans. Safety, durability, economic viability, and operational management challenges intensify rapidly with increasing span lengths, posing unprecedented technical barriers [3–5].

As the span increases, cable-stayed bridges face several constraints: (1) the sag effect caused by the self-weight of the stay cables reduces efficiency [6]; (2) the main girder's large axial force leads to a significant P-Δ effect, endangering structural stability [7]; (3) the

stability of cantilever construction is compromised [8]; and (4) the instability risks of both the main girder and the pylon become prominent [9]. Likewise, suspension bridges encounter bottlenecks with increasing span lengths, as wind stability decreases, and the economic and construction challenges of large anchorages in complex geological conditions become significant [10,11].

In this context, the HCSS bridge emerged as an innovative structure combining the advantages of both systems. It achieves a significant performance leap over traditional bridges by improving structural stability, stiffness, and span capacity, while reducing pylon height and anchorage requirements [12–16]. Although the concept dates back to the 19th century, technological limitations delayed its prominence until recent years, when HCSS bridges gained recognition in major world-class projects [1,17–21]. For example, the Third Bosphorus Bridge, with a 1408 m span, showcases the exceptional capabilities of HCSS bridges. Meanwhile, domestic projects like the Tongling and Xihoumen bridges signify the rise of HCSS bridges in China, where they are now central to engineering practice.

The design and analysis of HCSS bridges have a long history, with early investigations providing a strong foundation for contemporary practice [19,22–27]. However, as technology advances rapidly, new challenges emerge. Specifically, the transition zone, where the cable-stayed and suspension systems intersect, has garnered attention due to its stiffness discontinuity. This discontinuity is especially pronounced under live loads, leading to increased internal forces and deformation in the main girder [26,28]. Additionally, the lack of sufficient design data complicates the determination of optimal design parameters in specific HCSS bridge projects. Consequently, conducting full-bridge parameter analyses to assess the sensitivity of structural performance to various parameters and guiding the design process have become crucial issues requiring prompt attention.

Kamil Korus et al. [29] used an open-source visual programming language (VPL) for civil engineering, Dynamo, to generate scripts and establish a finite element model of an arch bridge. They applied a genetic algorithm for the parameter optimization of the model, significantly reducing the time consumed compared to traditional design iterations, and the method is applicable to other structures. Majid Pouraminian et al. [30] first generated a finite element model of the arch bridge using MATLAB, then optimized the construction process using the gradient-based Simultaneous Perturbation Stochastic Approximation (SPSA) algorithm, with the total volume of the substructure as the objective function. The results showed that SPSA can be effectively applied to bridge shape optimization programs, and the shape optimization process can significantly reduce the structure's weight. However, research on parameter optimization methods for the design of the new HCSS system is still limited.

This study tackled these challenges by developing a finite element model of a double-pylon, three-span HCSS bridge with a main span of 1440 m to analyze the effects of parameters such as the ratio of sag-to-span, cable inclination ratio, stiffness of the main pylons, position of the steel–concrete composite section, stiffness of the main cables, and stiffness of the stay cables on the static performance of the HCSS bridge. Based on structural optimization design methods, the key structural parameters of the HCSS bridge are optimized and compared to the original design to evaluate the mechanical performance of the system. This research aimed to provide a scientific basis for optimizing the HCSS bridge design, thus promoting the continued advancement of bridge engineering technology.

2. Engineering Case Description

2.1. Bridge Information

The HCSS bridge represents a significant performance leap from traditional bridges by improving structural stability, stiffness, and spanning capacity. Additionally, it substantially reduces the need for tall towers and anchorage.

This study examined a combined road and railway bridge that features both cable-stayed and suspension designs, with a main span of 1440 m. The bridge utilizes a modified Dissing system, featuring a span arrangement of 375 m, 1440 m, and 375 m, with a total

deck width of 58 m. Three auxiliary piers are positioned at the side spans. The central section includes a double-track railway, flanked by four road lanes on either side. The primary beam configuration employs a hybrid beam structure. The main span consists of a steel box girder, measuring 6 m in height and 58.5 m in width, while the side spans consist of concrete girders, with a height of 5.5 m. The elevation of the bridge, along with the cross-sections of the central steel box girder and the side concrete girders, is illustrated in Figures 1–3, respectively. The key parameters of the bridge are summarized in Table 1.

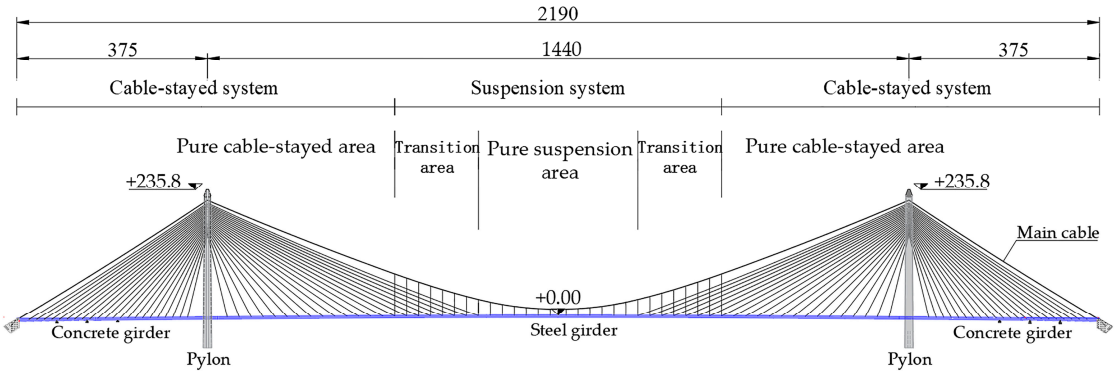


Figure 1. Structural diagram of the hybrid cable-stayed and suspension (HCSS) bridge system (unit: m).

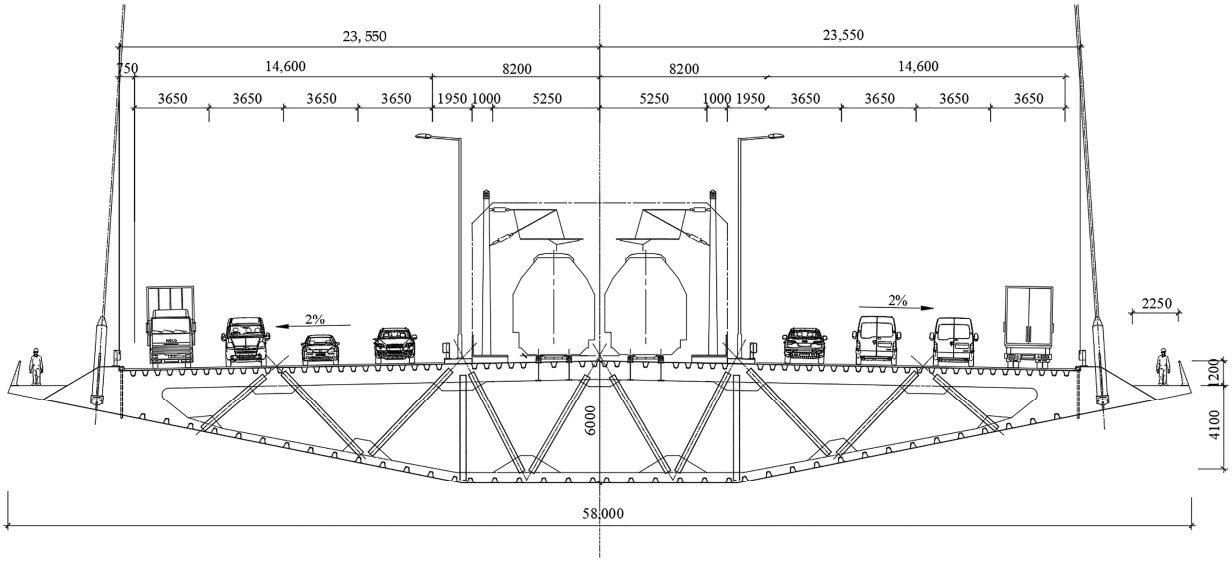


Figure 2. Standard cross-section of the mid-span steel box girder (unit: mm).

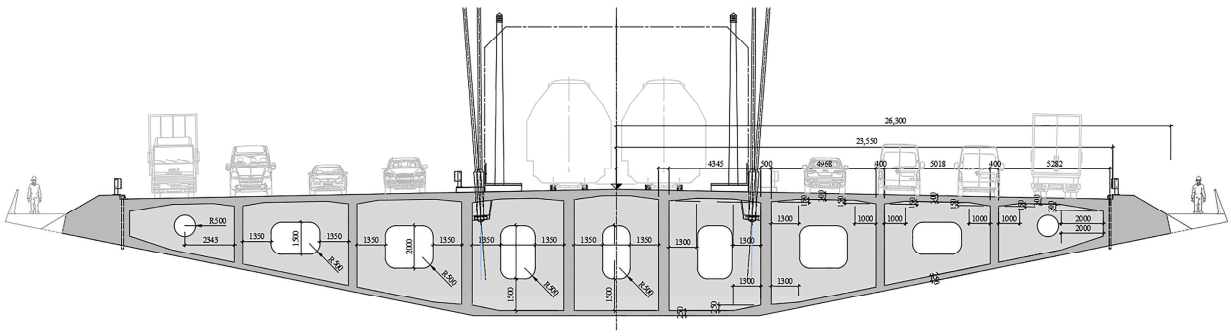


Figure 3. Standard cross-section of the edge span concrete beam (unit: mm).

Table 1. Key parameters of the entire bridge.

Parameter		Unit	Value
Span length	Left side span	m	375
	Main span	m	1440
	Right side span	m	375
Steel box girder	Material	-	Q345qD
	Area	m^2	3.307
Concrete box girder	Material	-	C60
	Area	m^2	56.648
Pylon	Material	-	C60
	Height	m	335
Main cable	Material	-	Steel
	Tensile strength	MPa	1860
Stay cable	Area	m^2	0.483
	Material	-	Steel
Hanger	Tensile strength	MPa	1860
	Material	-	Steel
	Tensile strength	MPa	1860

The cable system includes the main cables, stay cables, and hangers. The main cables consist of two strands, each made up of 127 wire ropes, with a rope diameter of 723 mm. The stay cables are arranged in a double-layer configuration with 22 pairs for both the main and side spans, spaced 16 m longitudinally along the girder and 2–3 m vertically along the pylons. The transition area measures 240 m in length. The bridge uses 32 pairs of hangers, 10 of which are located in the transition area, with a longitudinal spacing of 24 m along the girder. The numbering diagram of the mid-span stay cables and hangers is shown in Figure 4. Its cross-sectional area is shown in Figure 5.

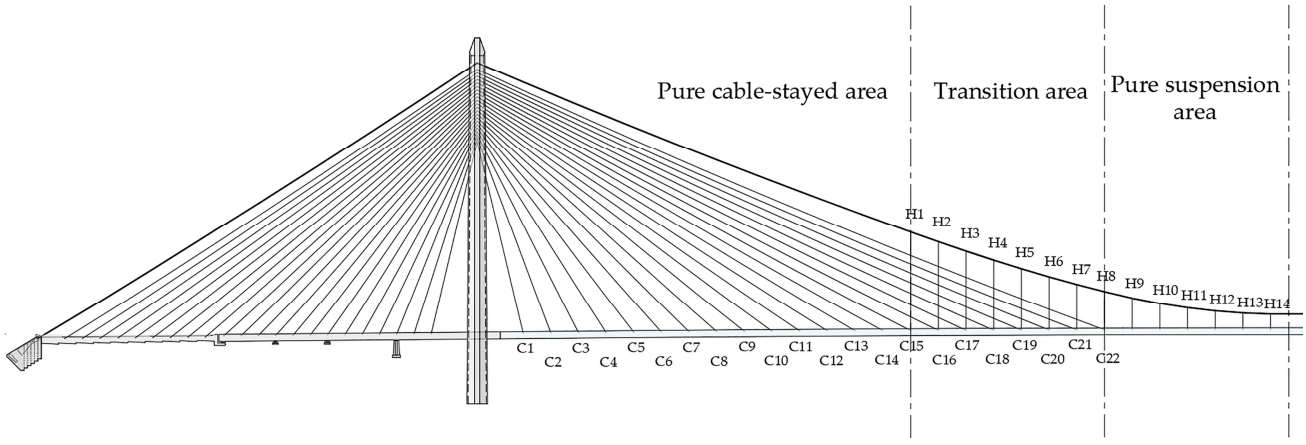


Figure 4. Numbering diagram of the mid-span half-span stay cables and hangers.

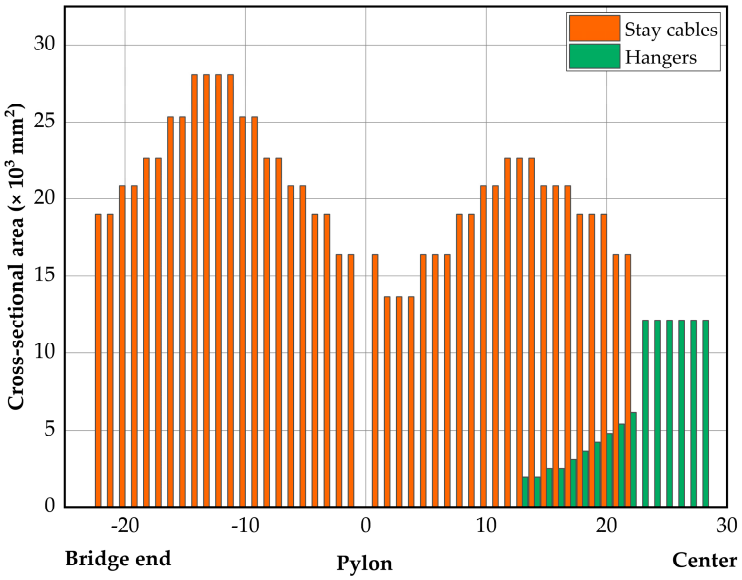


Figure 5. Cross-sectional areas of the stay cables and hangers.

2.2. Finite Element Model of the Bridge

The spatial geometric nonlinear finite element model used in this study was developed with the general-purpose finite element software ANSYS 2022 R1. In this model, three-dimensional truss elements (LINK10) simulate the cable system, designed to only experience tensile forces. The main girder and pylon are modeled with three-dimensional beam elements (BEAM4), and the main girder is represented as a single girder. Geometric nonlinear effects of the structure are considered during the calculation process. The spatial finite element model developed in this study is shown in Figure 6.

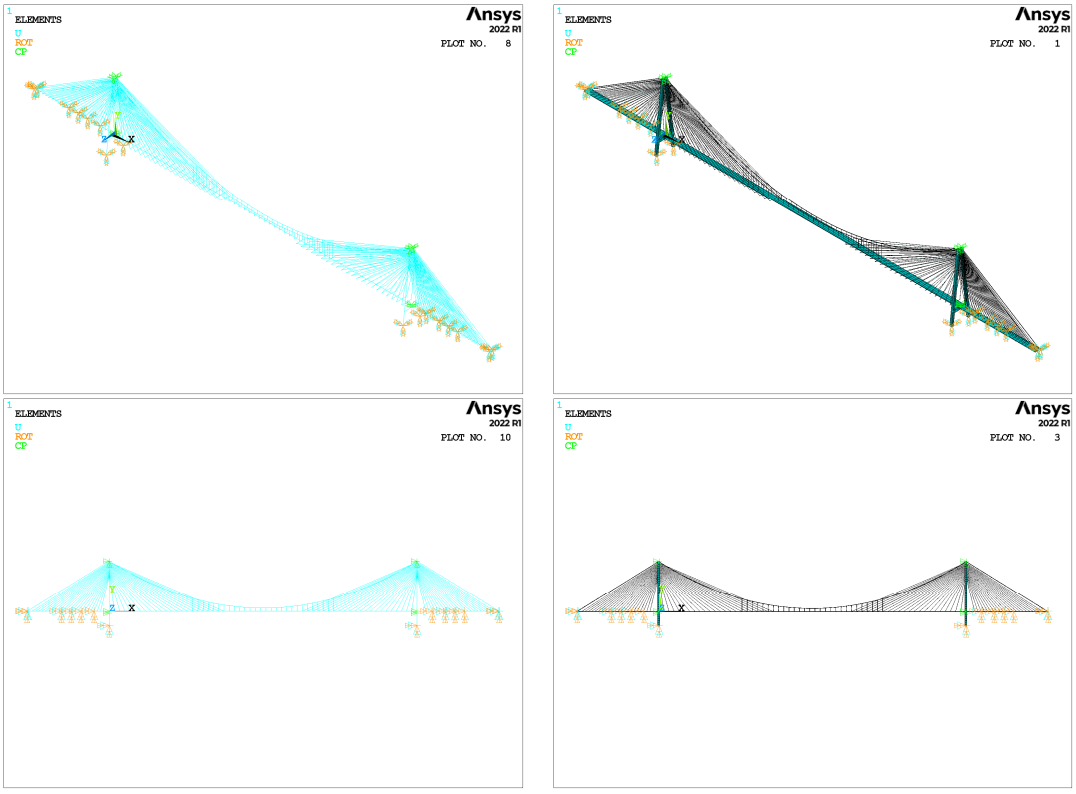


Figure 6. *Cont.*

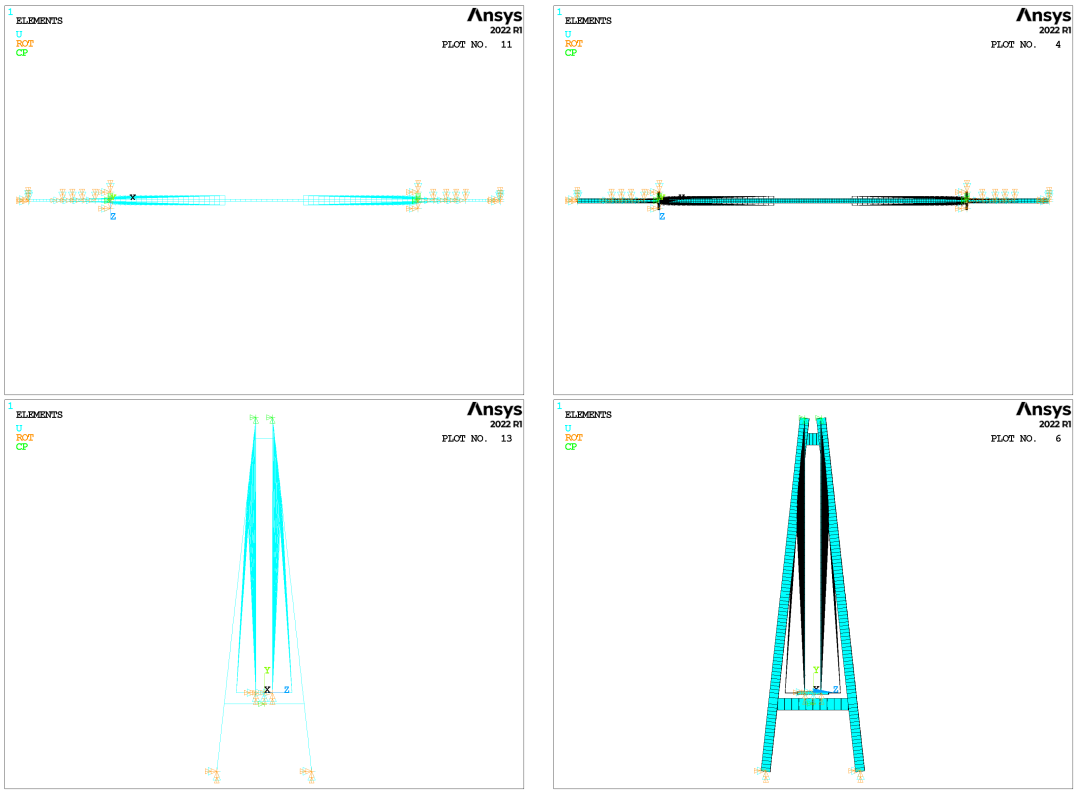


Figure 6. ANSYS spatial finite element model.

Due to the unique structure of the HCSS bridge system, a concrete box girder is used for the edge spans, while a steel box girder is used for the mid-span. The main girder and the bridge pylon are both made of steel. The specific elements and material properties used in this model are shown in Table 2, aligning with the actual engineering design values. In this setup, the mechanical properties of the LINK10 element are configured to allow only tensile forces (no compression), and its lateral stiffness is ignored. Both the main girder and the main tower are modeled using the BEAM4 element, which represent beam structures. For the material properties, classic constitutive models are applied for both concrete and steel.

Table 2. Parameters of the finite element model.

Structure	Element Type	Elastic Modulus (MPa)	Poisson's Ratio	Density (kg/m^3)
Main cable	LINK10	1.95×10^5	0.31	7850
Hanger	LINK10	1.95×10^5	0.31	7850
Stay cable	LINK10	1.95×10^5	0.31	7850
Steel main beam	BEAM4	2.10×10^5	0.3	7850
Concrete main beam	BEAM4	3.50×10^4	0.2	2500
Pylon	BEAM4	2.10×10^5	0.3	7850

Live loads in the finite element model are selected based on Chinese standards [31,32]. The vehicle load is defined as a Class I highway load, and the train load is specified as a ZK high-speed railway load, as shown in Figure 7. Each load is applied longitudinally to its corresponding lane.

The model in this study includes detailed boundary constraints, as specified in Table 3, consistent with the design drawings. In this context, the X direction represents the longitudinal axis of the bridge, Y denotes the vertical axis, and Z represents the transverse axis. In Table 3, the number 1 signifies a constrained direction, while 0 indicates an unconstrained direction.

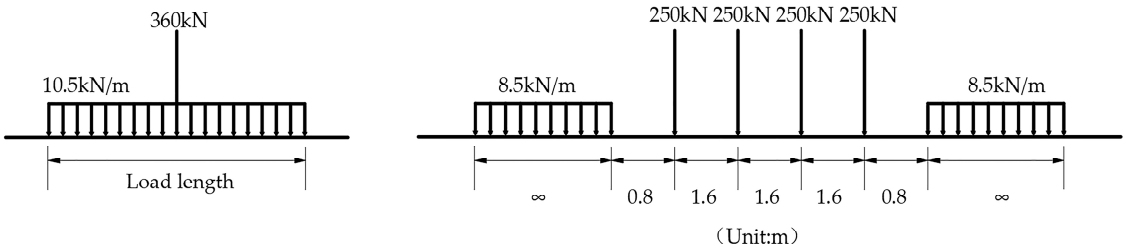


Figure 7. Live load schematic drawing for the global finite element model.

Table 3. Boundary constraints.

Position	DX	DY	DZ	ROTX	ROTY	ROTZ
Anchor node of the main cable	1	1	1	1	1	1
Bottom of the pylon	1	1	1	1	1	1
Abutment	1	1	0	0	0	0
Auxiliary pier	1	1	0	0	0	0
Main cable and pylon	1	1	1	1	1	1
Girder and pylon	1	1	0	0	0	0

In addition, this simulation experiment was conducted on a computer equipped with an Intel i7 12,700 processor and 16 GB of DDR4 memory, running the Windows 10 operating system. The simulation software used in the experiment was ANSYS 2022 R1.

2.3. Validation of the Finite Element Model

Figure 8 illustrates the bending moment diagram of the HCSS bridge under the action of self-weight in the completed state. As shown, the bending moments experienced by the main girder in different areas align with the distribution typically seen in continuous beams with rigid supports, and the overall values are relatively small. This suggests that the bending moments in the joint regions, calculated using this rigid support beam method, change smoothly, meeting the target for the final bridge state. Therefore, it can be concluded that the finite element model is reasonable.

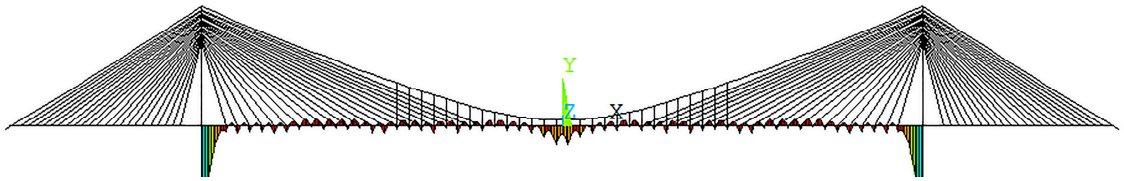


Figure 8. Bending moment diagram of the main girder in a reasonable final bridge state.

3. Optimization Design

3.1. General Process of the Optimization Design

This study uses the optimization module of the ANSYS 2022 R1 finite element software to optimize the design of the HCSS bridge. The core concept of optimization design is to identify the conditional extreme value of the objective function under constraints related to structural geometry and mechanical performance, thereby determining the optimal structural parameters. The optimization process involves several steps. First, key structural parameters are chosen as design variables. Second, during the optimization, specific performance requirements that the structure must satisfy are defined as state variables. Finally, based on these constraints, the design optimization seeks to minimize the objective function to achieve the desired results.

- Step 1: Create the Finite Element Analysis Model

Parameterized Modeling: In the pre-processor, initialize the design variables (DVs) and create a parameterized analysis model using these variables.

Loading and solving.

Extract Results and Assign Values: Extract the finite element analysis results through post-processing, then assign these values to the corresponding state variables (SVs) and objective function (OBJ).

- Step 2: Create Optimization Analysis File

Specify the Finite Element Results File: In the ANSYS optimization module (/OPT), specify the finite element results file for optimization analysis.

Declare Optimization Variables: Define the design variables, state variables, and objective function, including their upper and lower limits and convergence step sizes.

Select Optimization Tools and Methods: Choose the appropriate optimization tools and methods for the problem at hand.

Determine Iteration Control: Set the iteration control methods for the optimization process and initiate the analysis.

Evaluate Optimization Variables: Based on feedback from the optimization module's processor, compare the current optimization variables with those from the previous iteration to determine if the objective function has converged and met the target requirements.

- Step 3: Revise Design Variables

After completing the previous iteration, revise the design variables and perform the next iteration to achieve the optimized design results.

Figure 9 illustrates the specific flowchart of the ANSYS optimization design process described above.

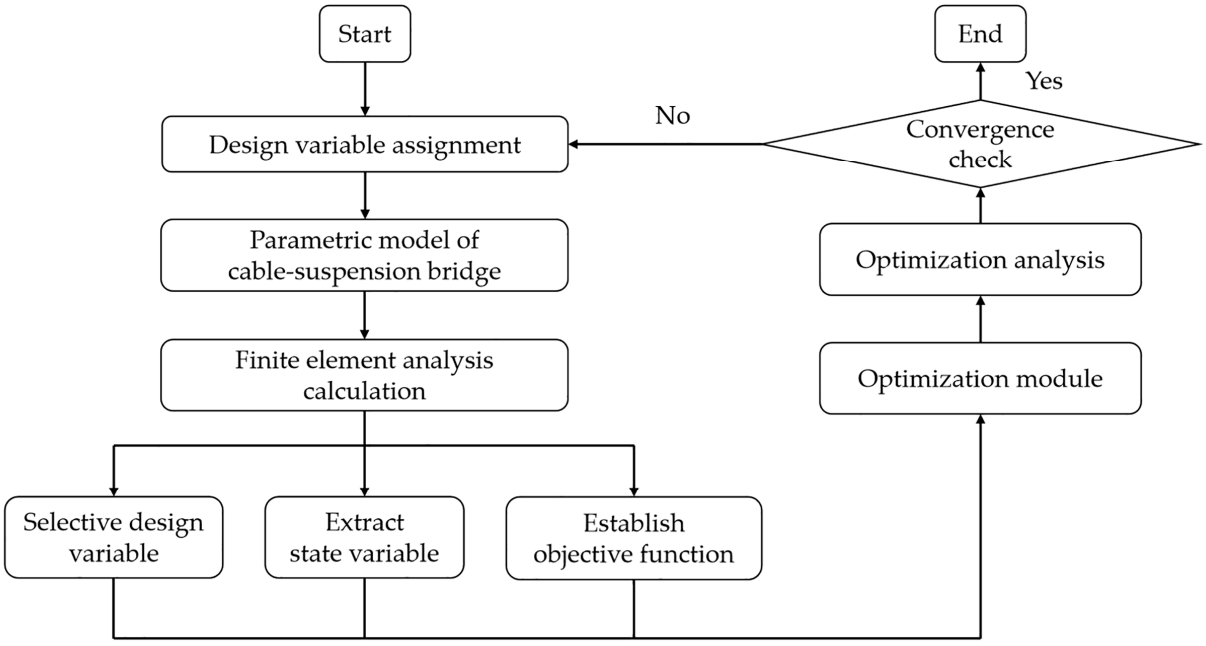


Figure 9. Flow chart of ANSYS optimization analysis [33].

3.2. Optimization Variable Settings

3.2.1. Design Variables

Based on prior research, this section analyzes the sensitive design parameters of HCSS bridges, primarily categorized into component material properties, geometric dimensions, and overall structural design parameters (e.g., sag-to-span ratio, inclined suspension ratio). Studies indicated that under identical strain conditions, variations in short hanger parameters have a negligible effect on structural forces [34]. The main girder parameters are typically fixed during the design process and thus not considered. Additionally, the steel-concrete interface between the side span and central span girders impacts the structural forces of the entire bridge. This factor requires consideration.

Therefore, this section selects the following parameters for the optimization of the HCSS bridge: span-to-depth ratio, cable-to-hanger ratio, pylon stiffness, stay cable stiffness, main cable diameter, stay cable diameter, and the position of the composite steel-concrete interface. The values of these design variables during the optimization process are specified in Table 4.

Table 4. Values of the design variables.

Design Variable	Parameter Name	Unit	Lower Limit of the Range	Upper Limit of the Range
Span-to-rise ratio	FL	-	0.125	0.163
Distance between stay cables	LC	m	20	40
Distance from stay cable to pylon	LTC	m	12	32
Elastic modulus of the pylon	ETO	MPa	8.20×10^4	3.71×10^5
Elastic modulus of the main cable	ES	MPa	8.40×10^4	3.36×10^5
Elastic modulus of the stay cables	EC	MPa	8.40×10^4	3.36×10^5
Diameter of the main cable	DS	m	0.5	1
Position of the steel-concrete interface	ND	-	0	30

The upper and lower limits of the variable values are based on traditional design schemes, which are derived from actual engineering projects [35–37].

3.2.2. State Variables

In the optimization process, the state variables include mid-span displacement, horizontal displacement at the top of the pylon, maximum force in the end hangers (H8), maximum force in the stay cables, bending moment at the base of the bridge pylon, and bending moment in the main beam within the suspension bridge area. Table 5 provides the state variables along with their corresponding upper and lower limits.

Table 5. State variables and their ranges.

State Variable	Parameter Name	Unit	Lower Limit of the Range	Upper Limit of the Range
Mid-span displacement	DY	m	−0.05	0
Horizontal displacement at the top of the pylon	UXT	m	−0.03	0.03
Maximum cable tension in the tail hangers H8	NC	kN	0	10,000
Maximum cable tension in the stay cables	NH	kN	0	30,000
Bending moment at the base of the bridge pylon	MT	MN·m	0	10,000
Bending moment of the main beam in the cable-stayed region	MZL	MN·m	−1000	1000

The upper and lower limits of the variable values are based on traditional design schemes, which are derived from actual engineering projects [35–37].

3.2.3. Objective Function

The deformation of the main girder in the completed bridge state is taken as the primary focus of investigation. After applying a uniformly distributed load to the entire bridge, the objective function for the optimization process is established. Let the vertical displacement of the main girder node be u_{yi}, where i represents the node number of the main girder, and the structural displacement objective function is defined as

$$f(x) = \sum_{i=1}^{n} {u_{yi}}^2 \quad (1)$$

The goal of the optimization design is achieved by minimizing the extremum of the objective function.

3.3. Optimization Method

Two primary optimization methods are used in the ANSYS optimization module: the zero-order and first-order optimization methods.

1. Zero-Order Optimization Methods: These methods utilize function approximation for optimization and are primarily applied in preliminary optimization stages. Zero-order methods are suitable for most engineering problems because they do not require gradient information and are computationally less intensive.
2. First-Order Optimization Methods: These methods offer a more precise optimization analysis. These methods involve computing the first-order partial derivatives of state variables and objective functions concerning the design variables. Gradient-based optimization techniques are then applied to analyze and optimize these derivatives.

In this study, both methods are employed to ensure the accuracy of the optimization process. The optimization control settings are summarized in Table 6.

Table 6. Optimization method control table.

	Zero-Order Optimization Method	First-Order Optimization Method
Maximum number of iterations	50	50
Variation degree of linear search step size range (%)	-	5
Variation degree of gradient calculation for design variable range (%)	-	0.1

3.4. Optimization Validation

To ensure reliable optimization results, three distinct sets of initial design variable values were employed in the optimization process. These values were sourced from traditional design schemes, key structural parameter analysis in Section 2, and randomly generated values. Table 7 presents the initial values and final optimization results for the three sets of design variables. Figure 10 illustrates the relationship between the objective function and the number of iterations during the optimization process.

Table 7 shows that the objective function approaches a stable value. All three sets of design variable values converge to generally consistent optimized results. Hence, the structural optimization design using ANSYS is demonstrated to be feasible.

Table 7. Summary of optimization results.

Design Variable	Conventional Design Scheme		Parameter Analysis Scheme		Random Acquisition Scheme	
	Initial Value	Optimized Value	Initial Value	Optimized Value	Initial Value	Optimized Value
Span-to-rise ratio (m)	0.156	0.152	0.149	0.151	0.201	0.154
Distance between stay cables (m)	24	24	28	24	30	24
Distance from stay cable to pylon (m)	24	24	32	24.6	50	23.9
Elastic modulus of the pylon (MPa)	2.06×10^5	2.07×10^5	1.85×10^5	2.05×10^5	2.12×10^5	2.06×10^5
Elastic modulus of the main cable (MPa)	2.10×10^5	2.11×10^5	2.52×10^5	2.12×10^5	2.20×10^5	2.09×10^5
Elastic modulus of the stay cables (MPa)	2.10×10^5	2.01×10^5	1.89×10^5	2.18×10^5	1.90×10^5	2.14×10^5
Diameter of the main cable (m)	0.784	0.794	0.8	0.801	1.021	0.795
Position of the steel-concrete interface	10	12.2	8	11.6	16	12.5

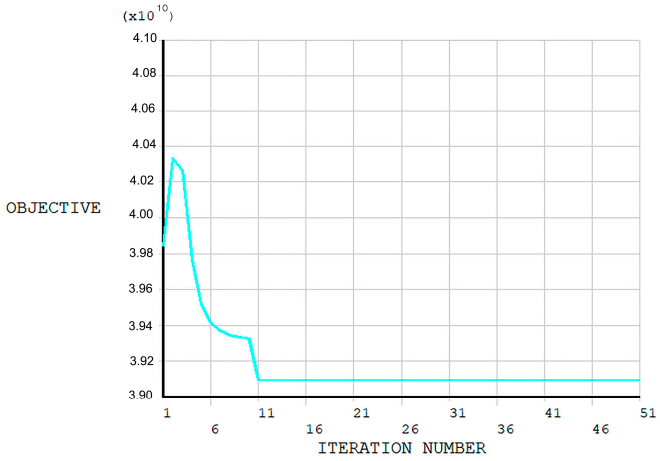


Figure 10. Curve of the objective function variation with the number of iterations.

4. Parameter Analysis

This study primarily focused on the final equilibrium state of the completed HCSS bridge and investigated the impact of various parameters on its static performance. As a result, the effects of construction stages, including cable tensioning and prestressing, are excluded from this analysis.

To determine the optimal bridge structure for its completed state, rigidity support reactions in the transition areas are allocated in a 1:1 ratio according to the forces in the stay cables and hangers. This study selected six key parameters—span-to-rise ratio, the cable-to-hanger ratio, pylon stiffness, steel-concrete interface position, and the stiffness of the main cables and stay cables—based on existing research to investigate their effects on the static performance of the HCSS bridge.

4.1. Impact of the Span-to-Rise Ratio

In an HCSS bridge, the span-to-rise ratio is defined as the ratio of the sag of the main cable to the length of the main span. The span-to-rise ratio is varied by adjusting the height of the pylons while keeping other parameters and load conditions unchanged. This analysis examined the response of key structural locations under different span-to-rise ratios, as illustrated in Figure 11.

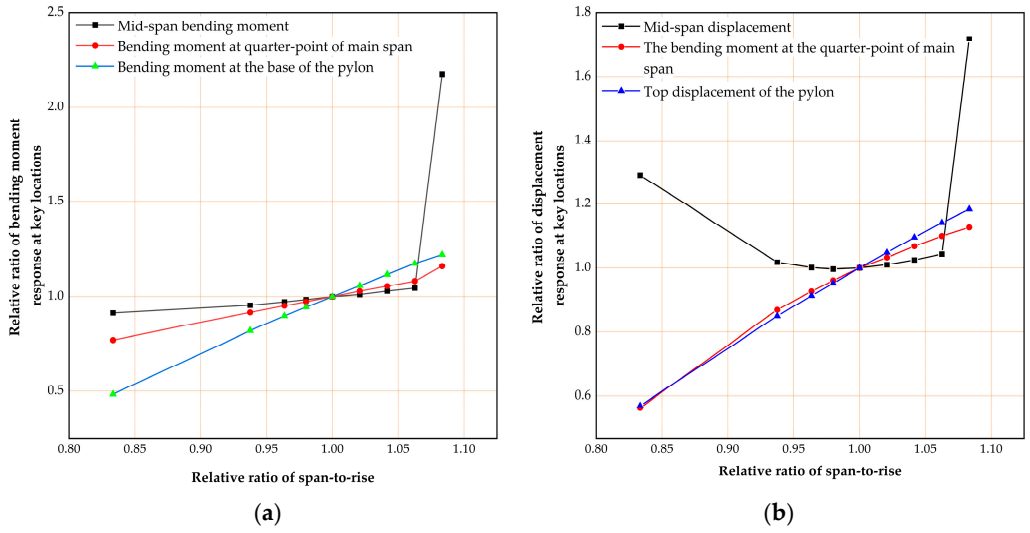


Figure 11. Impact of span-to-rise ratio on structural static performance: (**a**) bending moment at key locations; (**b**) displacement response at key locations.

Figure 11 shows that as the span-to-rise ratio increases, the bending moment at the mid-span also increases gradually. An 11% increase in the span-to-rise ratio results in the mid-span bending moment doubling from its initial value. When the span-to-rise ratio varies by ±8% from its base value, the mid-span displacement changes only slightly. In contrast, a fluctuation of approximately ±11% in the span-to-rise ratio leads to a significant increase in mid-span displacement. This indicates that both excessively high and low span-to-rise ratios can adversely affect the mid-span forces of the main girder.

Additionally, as the span-to-rise ratio increases, the bending moments at the quarter points of main span, the pylon base, and the displacements all increase continuously. This indicates that the span-to-rise ratio significantly affects the forces experienced by the bridge pylons.

4.2. Impact of the Cable-to-Hanger Ratio

In this section, the cable-to-hanger ratio is defined as the ratio of the span of the cable-stayed portion (L_1) to the span of the pure suspension portion (L_2), as illustrated in Figure 12. The cable-to-hanger ratio represents the proportion of the two subsystems in the HCSS bridge. A higher cable-to-hanger ratio indicates a shift toward the cable-stayed system, whereas a lower ratio indicates a shift toward the suspension bridge system. To adjust the cable-to-hanger ratio, other parameters must be kept constant. This is achieved by adjusting the distance from the first stay cable to the pylon (S_1) and the spacing between stay cables (S_0), as detailed in Table 8. By varying the cable-to-hanger ratio, the responses of the structure at key force locations are obtained, as illustrated in Figure 13.

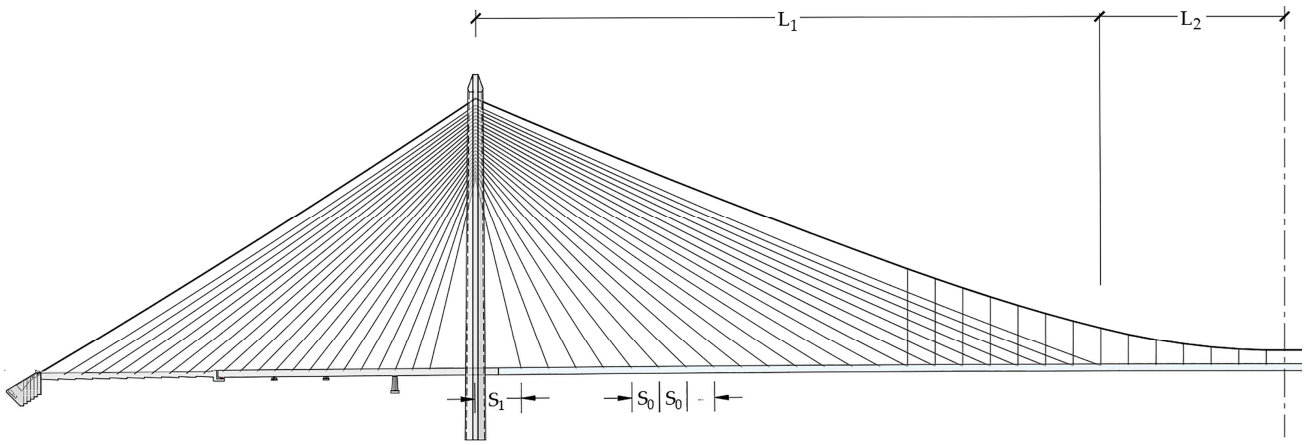


Figure 12. Schematic diagram of the cable-to-hanger ratio definition.

Table 8. Values of the cable-to-hanger ratio.

Distance Between Stay Cables S_0 (m)	Distance from First Stay Cable to Pylon S_1 (m)	Length of the Pure Cable-Stayed Area (m)	Length of the Pure Suspension Area (m)	Cable-to-Hanger Ratio
20	16	436	272	1.6
	24	444	264	1.68
	32	452	256	1.77
24	16	520	188	2.77
	24	528	180	2.93
	32	536	172	3.12
28	16	604	104	5.81
	24	612	96	6.38
	32	620	88	7.05

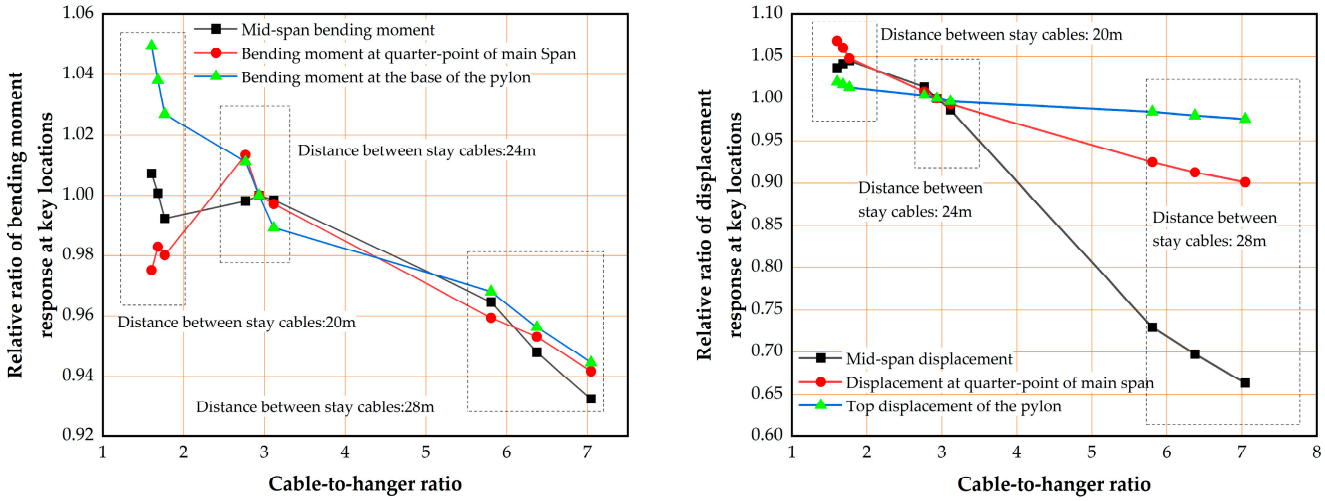


Figure 13. Impact of the cable-to-hanger ratio on structural static performance: (**a**) relative ration of bending moment response at key locations; (**b**) relative ration of displacement response at key locations.

Figure 13 shows that as the cable-to-hanger ratio increases, the bending moments at both the mid-span and quarter points decrease slightly, while the mid-span displacement of the main girder decreases by more than 30%. This indicates that increasing the proportion of the cable-stayed section enhances the overall stiffness and stability of the structure.

Additionally, as the cable-to-hanger ratio increases, the reductions in bending moments at the pylon base and displacements at the pylon top are relatively small.

The analysis indicates that increasing the proportion of the cable-stayed system has a minimal impact on the pylons but significantly enhances the stiffness and stability of the main girder.

4.3. Impact of Pylon Stiffness

This section adjusts the pylon stiffness indirectly by varying the elastic modulus of the pylon material. The resulting changes in internal forces and displacements at key locations in the structure are illustrated in Figure 14.

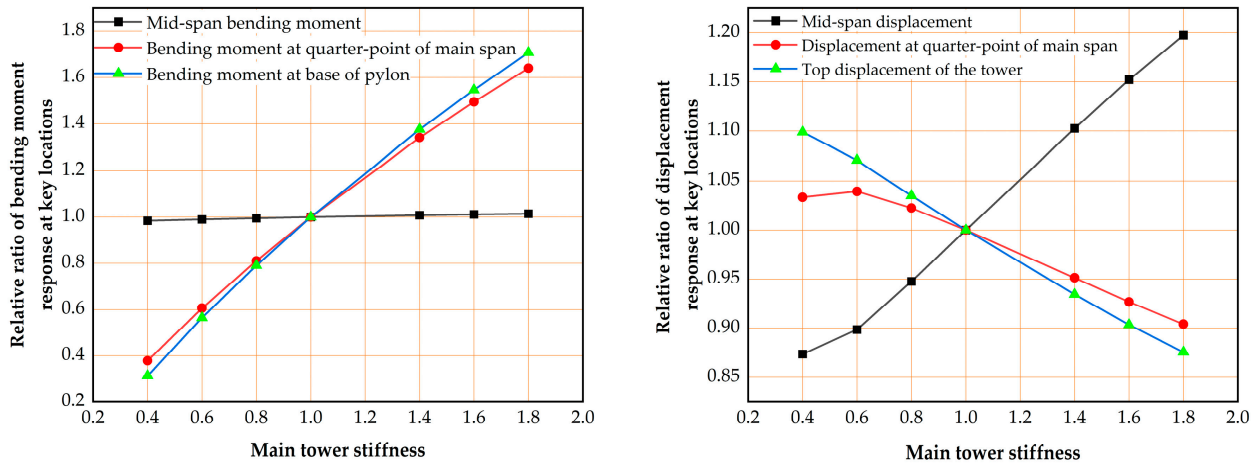


Figure 14. Impact of pylon stiffness on structural static performance: (**a**) relative ration of bending moment response at key locations; (**b**) relative ration of displacement response at key locations.

Figure 14 shows that as the pylon's flexural stiffness increases, the bending moment at the pylon base rises significantly, while the horizontal displacement at the pylon top decreases noticeably, which enhances the lateral resistance of the main girder. Although increasing the pylon's flexural stiffness minimally affects the mid-span bending moment of the main girder, it leads to a noticeable increase in mid-span displacement. Conversely, bending moments at the quarter points of the main span increase with stiffness, while displacements at both the quarter points and mid-span show opposite trends.

4.4. Impact of the Steel–Concrete Interface Position

To investigate the impact of the steel–concrete interface position on the HCSS bridge, this section varies the number of concrete beam segments (NCON) to adjust the steel–concrete interface position, as shown in Figure 15. The deformation and force responses at the key locations in the bridge for different steel–concrete interface positions are analyzed, as shown in Figure 16.

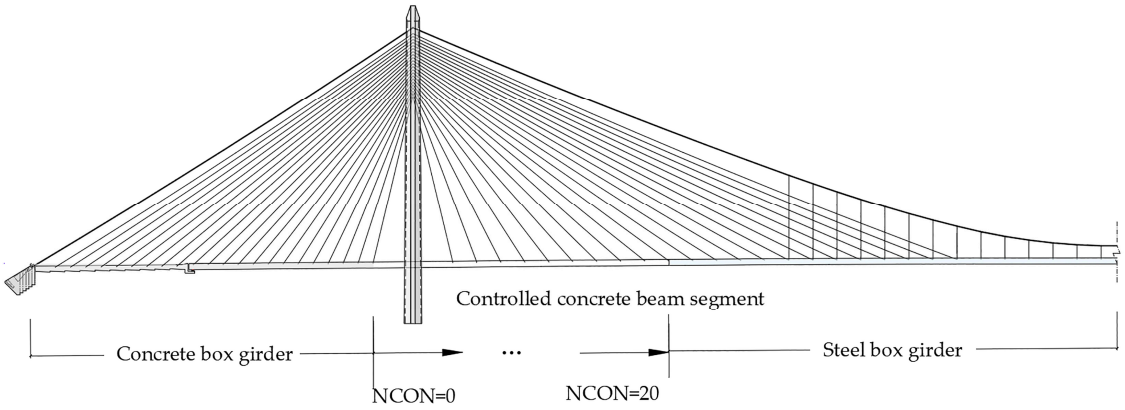


Figure 15. Schematic diagram of the steel–concrete interface position.

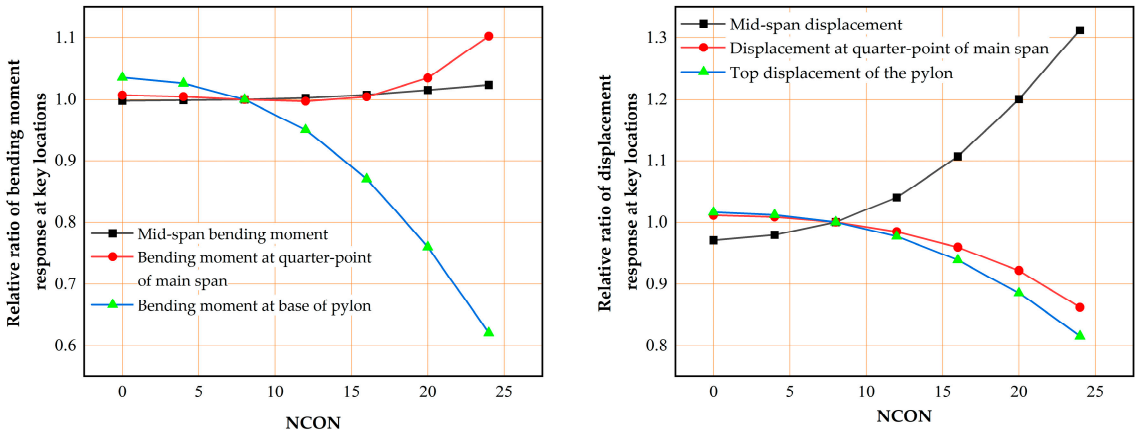


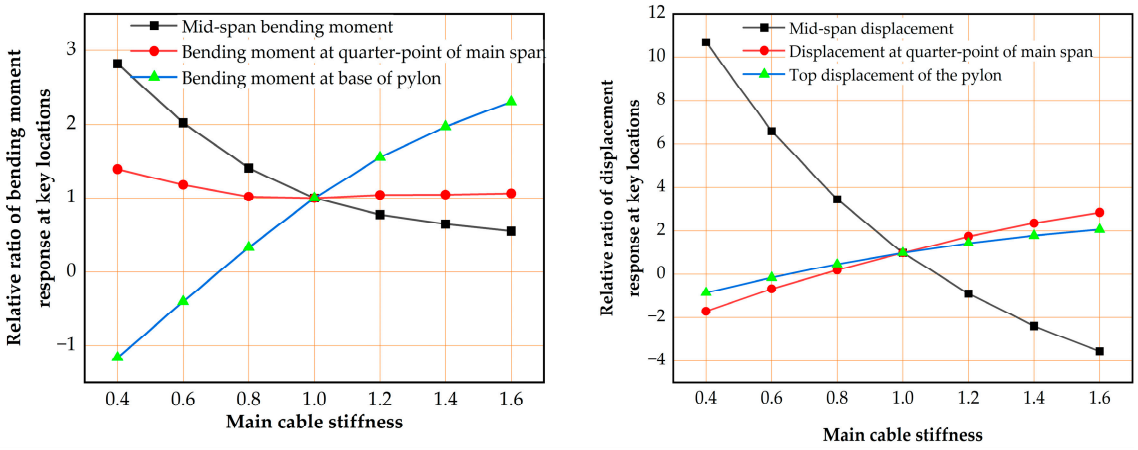
Figure 16. Impact of the steel–concrete interface on structural static performance: (**a**) relative ration of bending moment response at key locations; (**b**) relative ration of displacement response at key locations.

Figure 16 shows that as NCON increases, the bending moment at the pylon base and the horizontal displacement at the pylon top decrease. When no concrete beams are present in the main span, the changes are gradual; however, their addition leads to a significant reduction. The mid-span bending moment increases slowly, but with the introduction of concrete beams in the main span, the mid-span displacement increases dramatically, with the maximum change exceeding 30% of the design base value.

The above analysis indicates that while adding concrete beam segments in the main span enhances the overall stiffness of the bridge, it also increases the self-weight, which significantly affects the forces and deformations at the mid-span. Therefore, careful consideration is required when determining the number of concrete beam segments.

4.5. Impact of Main Cable Stiffness

In an HCSS bridge, variations in the main cable stiffness affect its deformation under constant loads, thereby influencing the forces and deformations in the pylons and girders. By varying the main cable stiffness parameters in the finite element model, the resulting changes in internal forces and displacements at key structural locations are illustrated in Figure 17.



(**a**) (**b**)

Figure 17. Impact of main cable stiffness on structural static performance: (**a**) relative ration of bending moment response at key locations; (**b**) relative ration of displacement response at key locations.

As shown in Figure 17, variations in the main cable stiffness have the most significant effect on the bending moment at the pylon base. When the main cable stiffness is reduced to 70% of the design value, the bending moment at the pylon base decreases to nearly zero. Conversely, when the main cable stiffness increases to 1.6 times the design value, the bending moment at the pylon base rises to 2.5 times its initial value, while the bending moment at the quarter points of the main girder remains relatively unchanged. This analysis indicates that the main cable stiffness has a substantial impact on the forces and deformations throughout the bridge.

4.6. Impact of Stay Cable Stiffness

Variations in stay cable stiffness affect cable elongation, adjust the deformation of the pylons and girders, and influence the overall bridge forces. In the transition area, stay cable stiffness affects the load distribution between cable-stayed and suspension bridge systems. This section varies the stay cable stiffness parameters to evaluate the resulting changes in internal forces and displacements at key structural locations, as shown in Figure 18.

As shown in Figure 18, increasing the stiffness of the stay cables leads to significant changes in the bending moments and displacements at the quarter points of main span, while the mid-span bending moment and displacement increase only slightly. The bending moment at the pylon base and the displacement at the pylon top remain nearly unchanged. This occurs because increased stay cable stiffness reduces the elastic elongation of the cables under the same load, thereby decreasing the sag. To counteract the upward displacement of the main girder caused by elastic elongation, larger bending moments and displacements at the mid-span are observed, especially when the main span consists of lightweight steel box girders. Conversely, at the quarter points of main span, reduced elastic elongation

results in increased positive displacements. The analysis indicates that increasing stay cable stiffness affects the structural forces, while it enhances overall stiffness, it must be applied judiciously to avoid adverse effects.

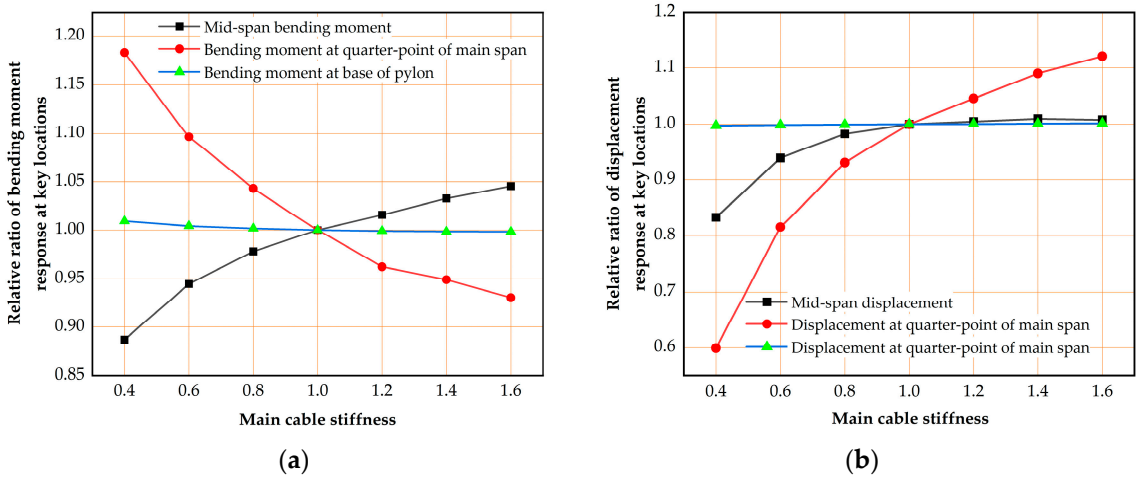


Figure 18. Impact of stay cable stiffness on structural static performance: (**a**) relative ration of bending moment response at key locations; (**b**) relative ration of displacement response at key locations.

5. Optimization Results

This section identifies the following parameters of the HCSS bridge as design variables: the span-to-rise ratio, the cable-to-hanger ratio, the stiffness of the pylon, the stiffness of the stay cables, the diameter of the main cable, the diameter of the stay cables, and the position of the steel–concrete interface. The mid-span displacement, the horizontal displacement at the top of the pylon, the maximum cable tension in the end hanger, the maximum cable tension in the stay cables, the bending moment at the base of the bridge pylon, and the bending moment of the main beam in the cable-stayed region are selected as state variables for the optimization design. A comparison of the forces in the stay cables, hanger, main beam, and structural stiffness characteristics before and after optimization was conducted.

5.1. Stay Cable Force Analysis

5.1.1. Effects of Dead Load

Under dead load, Figure 19 compares cable forces before and after optimization. Only the forces for half of the span are shown due to structural symmetry.

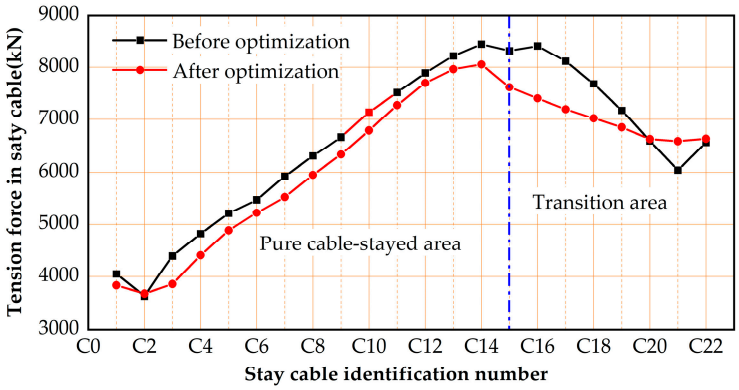


Figure 19. Cable forces under dead load.

Figure 19 shows that the cable forces are slightly reduced after optimization compared to before. In the transition area, the reduction in cable forces is more significant than in the pure cable-stayed area, and the changes are more gradual.

5.1.2. Effects of Dead and Live Loads

Figure 20 illustrates the cable forces and amplitudes under the combined effects of the dead load, vehicle load, and train load for the optimized scheme. Table 9 compares the maximum and minimum forces of the key cables before and after optimization.

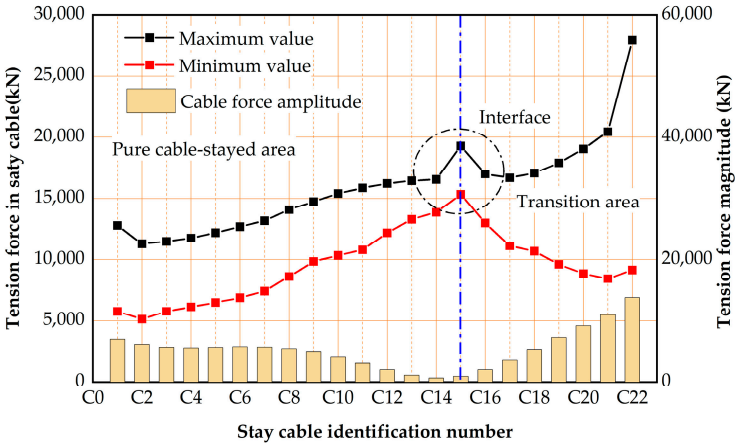


Figure 20. Cable forces under dead and live loads.

Table 9. Comparison of the key cable forces under dead and live loads.

	Before Optimization		After Optimization	
	Maximum Value	Minimum Value	Maximum Value	Minimum Value
Tension in the first stay cable (C1) near the pylon (kN)	15,142.8	8014.5	12,783.2	5762.1
Maximum tension in the stay cables (kN)	29,451.8	17,452.2	27,932.1	15,324.9
Tension in the end stay cable (C15) of the pure stay cable area (kN)	29,451.8	12,047.5	27,932.1	9156.7

Figure 20 and Table 9 show that under the combined effects of dead and live loads, maximum cable forces increase from the bridge pylon to the center span. Minimum cable forces rise in the pure cable-stayed region, peak at the boundary between the transition and pure cable-stayed regions, and then decrease. The amplitude of cable forces varies little in the pure cable-stayed region but increases significantly in the transition area, reaching 2.5 times the maximum value in the pure cable-stayed region. Additionally, cable forces at the start of the transition area (C15) and tail cables (C22), located at region boundaries, exhibit significant variations due to changes in stiffness. The maximum cable force in the tail cables is 27,932.1 kN, with an amplitude change of 13,775.4 kN, far exceeding other cables.

Optimization using ANSYS has led to substantial improvements in cable force distribution.

5.2. Hanger Force Analysis

5.2.1. Effects of Dead Load

Figure 21 compares hanger forces before and after optimization, while Table 10 compares the key hanger forces. Due to the bridge symmetry, results for only half of the hangers are shown.

Table 10. Comparison of key hanger forces under dead load.

	Before Optimization	After Optimization
Tension of the start hanger in the transition area (H1) (kN)	6866.6	5740
Tension of the tail hanger in the transition area (H8) (kN)	6138.9	5358.2
Tension in the start hanger in the pure suspension area (H9) (kN)	6844.8	7070.1
Tension in the mid-span hanger (H14) (kN)	8605.1	7593.8

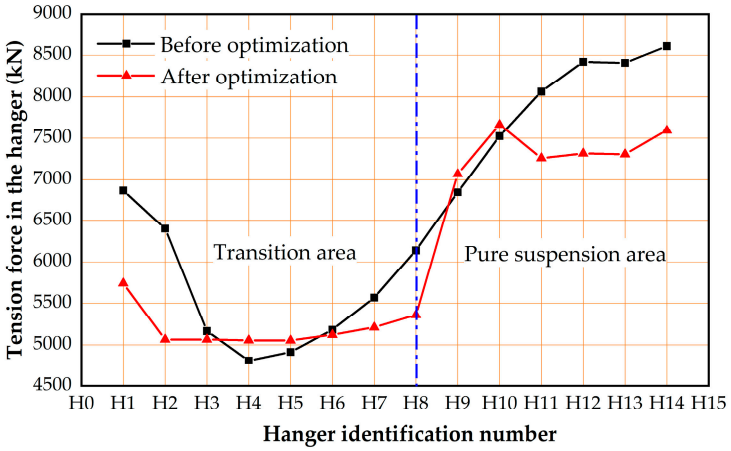


Figure 21. Hanger forces under dead load.

Figure 21 and Table 10 show that the internal forces in the hangers have significantly improved after optimization. The forces of the start hangers in the transition area (H1) decreased by 20%, tail hangers (H8) by 13%, and the average force in the pure suspension area by approximately 1000 kN. Compared to before optimization, the optimized scheme provides a more uniform variation of hanger forces within the transition area, though higher forces remain at the transition area ends. Noticeable step changes in internal forces occur when moving from the transition area to the pure suspension area, attributed to variations in structural stiffness.

5.2.2. Effects of Dead and Live Loads

Figure 22 presents the envelope of hanger forces and force amplitudes for the optimized scheme under dead and live loads. Table 11 compares the maximum and minimum hanger forces of key hangers before and after optimization.

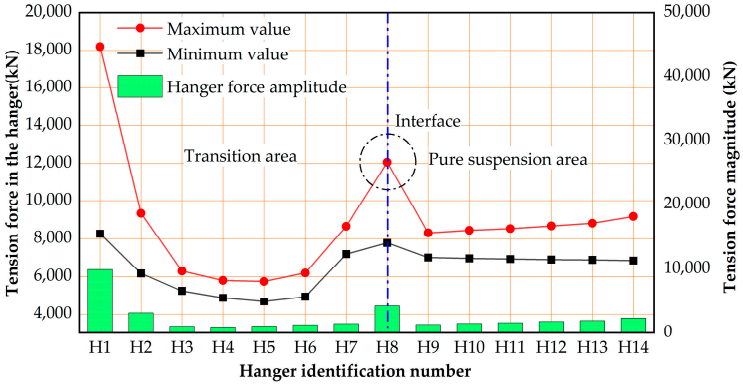


Figure 22. Hanger forces under dead and live loads.

Table 11. Comparison of key hanger forces under dead and live loads.

	Before Optimization		After Optimization	
	Maximum Value	**Minimum Value**	**Maximum Value**	**Minimum Value**
Tension in the start hanger in the transition area (H1) (kN)	20,248.9	14,024.8	18,200.9	10,730.2
Tension in the tail hanger in the transition area (H8) (kN)	15,142.3	11,047.7	12,066.1	7773.5
Tension in the start hanger in the pure suspension area (H9) (kN)	12,415.3	10,471.2	9166.6	6842.8

Figure 22 and Table 11 reveal that under the combined effects of dead and live loads, the maximum forces in start hanger (H1) and tail hanger (H8) are relatively high. Specifically, the force in H1 is twice that of H2, and the force in H8 exceeds that of H7 and H9 by 45%. Significant jumps in hanger forces occur at the boundaries between the pure cable-stayed area, transition area, and pure suspension area, due to large differences in structural stiffness. Within each region, the maximum and minimum hanger forces and their amplitudes exhibit minor variations. This analysis suggests that despite some larger hanger forces resulting from uneven stiffness changes, the hanger force distribution has significantly improved through structural parameter optimization.

5.3. Main Beam Force Analysis

To fully assess the mechanical performance of the main beam, this section analyzes the forces acting on it. Due to the bridge's symmetry, only the half from the edge span to the center span is considered.

5.3.1. Axial Forces

Figure 23 shows the axial forces in the main beam under dead load for the optimized scheme.

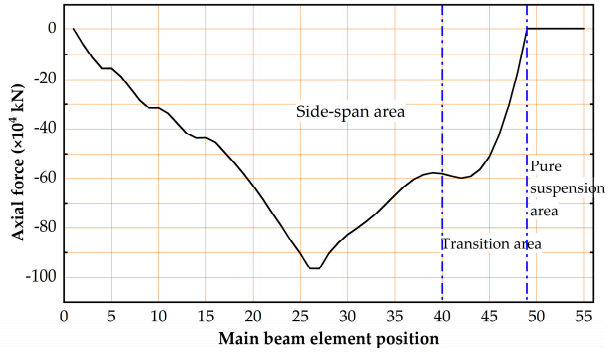


Figure 23. Axial forces in the main beam under dead load.

As the main beam moves from the edge span to the bridge pylon, the axial force increases and remains compressive, peaking at nearly 1000 MN at the bridge pylon. From the bridge pylon to the center span, the compressive force decreases, and the main beam experiences negligible compression in the pure suspension area.

Figure 24 shows the envelope of axial forces in the main beam under the combined effects of dead and live loads. The minimum axial forces in the mid-span main beam follow a similar trend to those under dead load alone, with the beam in the pure suspension area experiencing negligible compression. With varying live load combinations, the mid-span main beam may uniformly experience tension across its entire span, with values below 100 MN.

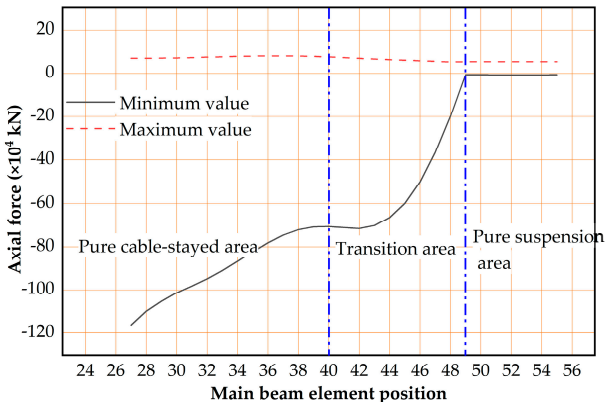


Figure 24. Axial forces in the mid-span main beam under dead and live loads.

5.3.2. Bending Moments

Figure 25 displays the envelope of the bending moments in the mid-span main beam under dead and live loads.

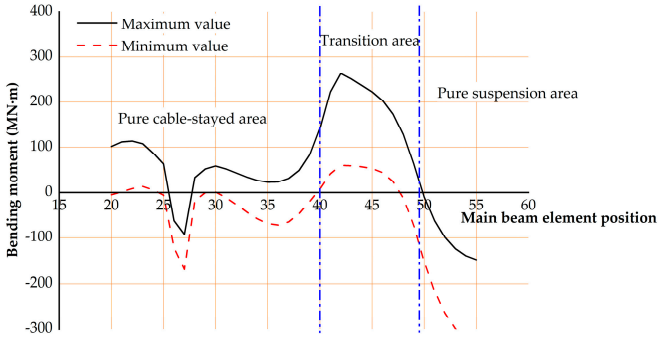


Figure 25. Bending moments in the mid-span main beam under dead and live loads.

The figure shows that under the combined effects of dead and live loads, the bending moment in the main beam within the pure cable-stayed area varies slightly, within ±100 MN·m. In contrast, in the transition and pure suspension areas, the bending moment varies significantly, with values ranging from 260 MN·m to −150 MN·m.

Under the combined dead and live loads, the lower edge of the main beam at mid-span in the pure suspension area experiences tension. Due to the structural stiffness variation between the transition area and the pure suspension area, bending moments show significant variation, with the maximum tensile moment exceeding 300 MN·m.

5.4. Structural Stiffness Characteristics

Table 12 compares the end rotations and displacements of the structure under three different conditions. Figures 26 and 27 display the envelopes of vertical and longitudinal displacements, respectively, under the combined effects of dead load, vehicle load, and train load for the optimized structure. Due to structural symmetry, only half of the main beam's deformation is shown.

Table 12. Comparison of structural displacements.

Live Load Type	Vertical Displacement (mm)		Longitudinal Displacement (mm)		End Rotation of Beam (10^{-3} rad)	
	Before Optimization	After Optimization	Before Optimization	After Optimization	Before Optimization	After Optimization
Static live load from vehicles	716.3	701.2	336.1	300.2	0.8	0.7
Static live load from trains	919.3	889.2	1036.3	982.8	1.5	1.3
Combined live load from vehicles and trains	2247.2	2017.4	2590.8	2348.2	2.1	1.9

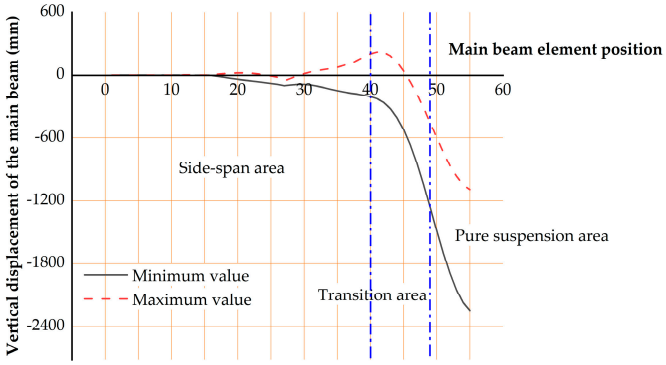


Figure 26. Envelope of vertical displacements in the main beam.

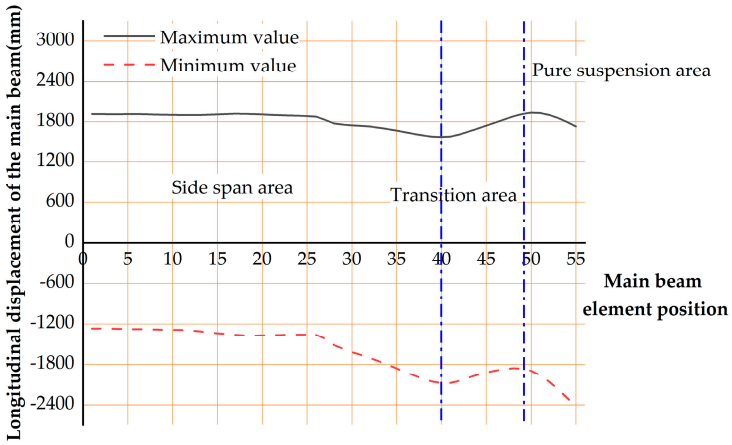


Figure 27. Envelope of longitudinal displacements in the main beam.

The figures and table show that optimizing the structural parameters of the HCSS bridge has reduced the main beam's deformation, indicating a significant improvement in the beam's stiffness. Under the combined effects of dead and live loads, the optimized structure exhibits the maximum vertical displacement of the main beam in the pure suspension area, with a downward deflection of 2247.2 mm. The deflection-to-span ratio is L/630, which is less than the L/500 specified by the standards [38], thus meeting the requirements.

Figures 26 and 27 show that the vertical deflection and longitudinal displacement curves of the main beam are relatively smooth from the edge span to the pure cable-stayed area. However, as the structure transitions from the pure cable-stayed area to the transition area, the displacement curves exhibit noticeable fluctuations. Specifically, the vertical displacement of the main beam reaches a maximum upward deflection in the transition area and a maximum downward deflection in the pure suspension area at mid-span, with a deflection difference of 1311 mm between these points. In the longitudinal displacement curve, both the maximum and minimum values display distinct extrema at the boundaries of the transition area, indicating non-smooth displacement in these areas due to varying stiffness.

6. Conclusions

Based on the design of a 1440 m main span HCSS bridge, this study developed a finite element model to investigate the mechanical performance of the system under dead and live loads. This study examines the effects of various parameters on the HCSS bridge's mechanical performance, such as the span-to-depth ratio, cable-to-hanger ratio, main cable tensile stiffness, stay cable tensile stiffness, and the bending stiffness of the pylon. Additionally, the study utilizes the zero-order and first-order optimization methods in ANSYS's optimization module to optimize parameters such as the span-to-depth ratio, stay cable spacing, pylon stiffness, main cable stiffness, stay cable stiffness, main cable diameter, and the position of the composite steel–concrete interface. The findings offer valuable insights into the HCSS bridge's performance in real-world engineering scenarios.

Based on this study, the following conclusions can be drawn:

- Both excessively large or small span-to-depth ratios negatively affect the forces acting on the mid-span of the main girder, with an increase in the span-to-depth ratio having a significant impact on the forces exerted on the bridge pylon. Increasing the spacing of the stay cables to enhance the cable-to-hanger ratio can significantly improve the stiffness and stability of the main girder structure, with minimal impact on the overall performance of the bridge pylon. While adding a certain number of concrete girder segments to the main span can enhance the overall stiffness of the bridge, it also increases the self-weight, significantly influencing the forces and deformations at the mid-span. As the main load-bearing component of the HCSS bridge, the stiffness

of the main cable has a critical impact on the forces and deformations of the bridge. Increasing the stiffness of the stay cables can improve the overall stiffness of the bridge, but beyond a certain point, this may have a detrimental effect on the structural forces.

- Optimizing relevant parameters for the stay cables in the transition area leads to a slight reduction in cable forces within the pure cable-stayed area, while the internal forces in the transition area exhibit more uniform and gradual changes. Under both dead and live loads, the cable force amplitude at the boundary between the pure cable-stayed region and the transition area is considerable, showing a significant increase within the transition area. The maximum cable force amplitude in the transition area is approximately 2.5 times greater than that in the pure cable-stayed area, and the force amplitude at the boundary between different regions significantly surpasses that of other stay cables.
- Under dead load conditions, optimizing the relevant parameters has significantly improved the internal forces in the hangers. Specifically, the forces in the end hangers of the transition area decreased by approximately 20%, while the forces in the tail hangers decreased by about 13%. Under the combined effects of dead and live loads, noticeable abrupt changes occur in the hanger forces at the boundaries between different regions, while the force amplitudes within each region exhibit minimal variation. Optimizing the structural parameters has led to a marked improvement in the force distribution of the hangers.
- Under dead load conditions, the axial force in the main beam increases continuously from the edge span to the bridge pylon, reaching a maximum of approximately 1000 MN at the pylon. In the pure suspension area at the mid-span, the main beam is essentially not subjected to compression. Under the combined effects of dead and live loads, the mid-span main beam experiences relatively uniform tensile forces across its entire span as load combinations vary. In the transition area, under combined dead and live loads, the bending moments in the main beam exhibit significant variations over a relatively small range with noticeable abrupt changes. Optimizing structural parameters has led to improvements in the force state and deformation of the main beam.
- The transition of the main beam from the edge span to the pure cable-stayed area is smooth in terms of structural stiffness. However, in the transition area, the displacement curve exhibits significant fluctuations, indicating variations in stiffness. Optimizing key structural parameters has reduced the main beam's deformation, leading to noticeable improvements in its force state and deformation characteristics.

This paper conducts a systematic analysis of the static performance of hybrid cable-stayed and suspension (HCSS) bridges. However, as a representative of large-span cable-supported special bridge types, HCSS bridges' wind resistance performance requires further investigation to fully comprehend their mechanical properties. Additionally, conducting studies on their dynamic performance is essential, as it is a significant aspect of their overall mechanical behavior.

Author Contributions: Conceptualization, Z.P. and L.J.; form analysis, Z.P. and L.J.; data curation, J.X., K.L. and H.P.; formal analysis, Z.P. and L.J.; funding acquisition, H.P.; investigation, Z.P. and J.X.; methodology, Z.P., L.J. and H.P.; project administration, H.P.; software, J.X. and Z.P.; validation, Z.P., L.J. and H.P.; visualization, J.X., Z.P., K.L. and H.P.; writing—original draft, Z.P.; writing—review and editing, J.X, Z.P. and K.L. All authors have read and agreed to the published version of the manuscript.

Funding: This work was funded by the Jiangxi Provincial Department of Science and Technology, grant number 2024ZG002, and Jiangxi Provincial Department of Science and Technology, grant number 2023H0008.

Data Availability Statement: Some or all of the data, models, and code that support the findings of this study are available from the corresponding author upon reasonable request (the design scheme of the HCSS bridge and FE data).

Acknowledgments: The authors are greatly indebted to the anonymous reviewers for their valuable comments and suggestions, which helped in improving the overall quality of this manuscript greatly.

Conflicts of Interest: Author Huiteng Pei was employed by the company Jiangxi Communication Design and Research Institute Co., Ltd. The remaining authors declare that the research was conducted in the absence of any commercial or financial relationships that could be construed as a potential conflicts of interest.

References

1. Gimsing, N.J.; Georgakis, C.T. *Cable Supported Bridges: Concept and Design*; John Wiley & Sons: Hoboken, NJ, USA, 2011; ISBN 1-119-95187-9.
2. Mao, W.; Hu, X. Latest developments and prospects for long-span bridges in China. *Bridge Constr.* **2020**, *50*, 13–19.
3. Martins, A.M.B.; Simões, L.M.C.; Negrão, J.H.J.O. Optimization of cable-stayed bridges: A literature survey. *Adv. Eng. Softw.* **2020**, *149*, 102829. [CrossRef]
4. Li, H.; Ou, J. The state of the art in structural health monitoring of cable-stayed bridges. *J. Civ. Struct. Health Monit.* **2016**, *6*, 43–67. [CrossRef]
5. Wang, D.; Ye, J.; Wang, B.; Wahab, M.A. Review on the service safety assessment of the main cable of long-span multi-tower suspension bridges. *Appl. Sci.* **2021**, *11*, 5920. [CrossRef]
6. Kim, S.; Won, D.H.; Kang, Y.J. Ultimate behavior of steel cable-stayed bridges—I. Rational ultimate analysis method. *Int. J. Steel Struct.* **2016**, *16*, 601–624. [CrossRef]
7. Freire, A.M.S.; Negrão, J.H.O.; Lopes, A.V. Geometrical nonlinearities on the static analysis of highly flexible steel cable-stayed bridges. *Comput. Struct.* **2006**, *84*, 2128–2140. [CrossRef]
8. Yoo, H.; Choi, D.H. Improved system buckling analysis of effective lengths of girder and tower members in steel cable-stayed bridges. *Comput. Struct.* **2009**, *87*, 847–860. [CrossRef]
9. Nicoletti, V.; Quarchioni, S.; Tentella, L.; Martini, R.; Gara, F. Experimental tests and numerical analyses for the dynamic characterization of a steel and wooden cable-stayed footbridge. *Infrastructures* **2023**, *8*, 100. [CrossRef]
10. Zhang, W.M.; Ge, Y.J.; Levitan, M.L. Aerodynamic flutter analysis of a new suspension bridge with double main spans. *Wind Struct.* **2011**, *14*, 187–208. [CrossRef]
11. Zhang, L.; Xiao, R.; Sun, B.; Jiang, Y.; Zhang, X.; Zhuang, D.; Zhou, Y.; Tu, X. Study on economic performances of multi-span suspension bridges—Part 1: Simple estimation formulas. *Struct. Eng. Mech.* **2013**, *47*, 265–286. [CrossRef]
12. Bruno, D.; Greco, F.; Lonetti, P. A parametric study on the dynamic behavior of combined cable-stayed and suspension bridges under moving loads. *Int. J. Comput. Methods Eng. Sci. Mech.* **2009**, *10*, 243–258. [CrossRef]
13. Konstantakopoulos, T.G.; Michaltsos, G.T. A mathematical model for a combined cable system of bridges. *Eng. Struct.* **2010**, *32*, 2717–2728. [CrossRef]
14. Qiu, J.; Shen, R.L.; Li, H.G.; Zhang, X. Analysis of structural parameters of cable-stayed suspension bridges. *Adv. Mater. Res.* **2010**, *163–167*, 2068–2076. [CrossRef]
15. Zhang, X.-J. Investigation on mechanics performance of cable-stayed-suspension hybrid bridges. *Wind Struct.* **2007**, *10*, 533–542. [CrossRef]
16. Starossek, U. Cable-stayed bridge concept for longer spans. *J. Bridge Eng.* **1996**, *1*, 99–103. [CrossRef]
17. Paultre, P.; Proulx, J.; Begin, T. Dynamic investigation of a hybrid suspension and cable-stayed bridge. *Earthq. Eng. Struct. Dyn.* **2000**, *29*, 731–739. [CrossRef]
18. Erdog, H.; Gülal, E. Ambient vibration measurements of the Bosphorus suspension bridge by total station and GPS. *Exp. Tech.* **2013**, *37*, 16–23. [CrossRef]
19. Sun, B.; Cai, C.; Xiao, R. Analysis strategy and parametric study of cable-stayed-suspension bridges. *Adv. Struct. Eng.* **2013**, *16*, 1081–1102. [CrossRef]
20. Lin, T.Y.; Chow, P. Gibraltar Strait crossing—A challenge to bridge and structural engineers. *Struct. Eng. Int.* **1991**, *1*, 53–58. [CrossRef]
21. Buckland, P.G. Increasing the load capacity of suspension bridges. *J. Bridge Eng.* **2003**, *8*, 288–296. [CrossRef]
22. Zhang, W.; Tian, G.; Chen, Y. Evolution of suspension bridge structural systems, design theories, and shape-finding methods: A literature survey. *J. Traffic Transp. Eng. (Engl. Ed.)* **2024**, *11*, 225–244. [CrossRef]
23. Reis, A.J.; Pedro, J.J.O. The Europe Bridge in Portugal: Concept and structural design. *J. Constr. Steel Res.* **2004**, *60*, 363–372. [CrossRef]
24. Arruda, M.R.T.; Serafim, J.P.M. Parametric test for the preliminary design of suspension bridges. *Int. J. Adv. Struct. Eng.* **2017**, *9*, 165–176. [CrossRef]
25. Zhang, W.; Chen, J.; Tian, G.; Chang, J. Reasonable completed state evaluation for hybrid cable-stayed suspension bridges: An analytical algorithm. *Structures* **2022**, *44*, 1636–1647. [CrossRef]
26. Xiao, L.; Huang, Y.; Wei, X. Study on deflection-span ratio of cable-stayed suspension cooperative system with single-tower space cable. *Infrastructures* **2023**, *8*, 62. [CrossRef]

27. Liang, T.; Zhao, H.; Liu, Y.-Q. Research on rational design of connection part for combined cable-stayed and suspension bridge. *J. Highw. Transp. Res. Dev.* **2016**, *33*, 70–75.
28. Wang, H.L.; Qin, S.F.; Huang, C.L.; Ge, X.M. Living load nonlinear analysis of self-anchored cable-stayed suspension bridges. *Appl. Mech. Mater.* **2010**, *29*, 1583–1587. [CrossRef]
29. Korus, K.; Salamak, M.; Jasiński, M. Optimization of Geometric Parameters of Arch Bridges Using Visual Programming FEM Components and Genetic Algorithm. *Eng. Struct.* **2021**, *241*, 112465. [CrossRef]
30. Pouraminian, M.; Azad, S.I.; sveučilište Sharif, T.; Ghaemian, M. Optimalizacija Oblika Lučnih Mostova s Otvorenim Nadlučnim Sklopom. *J. Croat. Assoc. Civ. Eng.* **2015**, *67*, 1177–1185. [CrossRef]
31. CCCC Highway Consultants Co., Ltd. *JTG-D60-2015*; General Specifications for the Design of Highway Bridges and Culverts. China Communications Press: Beijing, China, 2015.
32. National Railway Administration of People's Republic. *TB10002-2017*; General Specifications for the Design of Railway Bridges and Culverts. China Railway Publishing House: Beijing, China, 2015.
33. Zhou, Q.S. *Parameters Analysis and Optimal Design for the Suspension Footbridge*; Zhejiang University: Hangzhou, China, 2007. (In Chinese)
34. Ye, Y.; Zhang, Z.; Xia, G. Nonlinear Stochastic Static Analysis of Long spanSelf-anchored Cable-stayed Suspension Bridge. *Wuhan Univ. Technol. (Transp. Sci. Eng.)* **2009**, *33*, 1076–1079. (In Chinese)
35. Xiao, R.C.; Luo, X.H.; Jia, L.J.; Dai, L.M.; Xue, E.L.; Zhu, L.D.; Xiang, H.F. Design Attempt of the Liaoding East Waterway Cable-Stayed and Suspended Collaboration System. In Proceedings of the 13th Annual Meeting of the Bridge and Structural Engineering Society of China; China Civil Engineering Society: Shanghai, China, 1998; pp. 89–96. (In Chinese)
36. Xiao, R.C.; Xiang, H.F. Mechanies characteristics and economie performancesstudy for cable stayed suspension bridges. *China Highw.* **1999**, *3*, 43–48. (In Chinese)
37. Jin, G.S.; Yang, Z.J.; Liu, Y.H. Analysis of Main Design Parameters of Cable Stayedand Suspension Combined System Bridge. *Highway* **2007**, *3*, 80–84. (In Chinese)
38. Ministry of Transport of the People's Republic of China. *JTG/T 3365-01-2020*; Specifications for Design of Highway Cable-Stayed Bridge. People's Transportation Publishing House: Beijing, China, 2020. (In Chinese)

Disclaimer/Publisher's Note: The statements, opinions and data contained in all publications are solely those of the individual author(s) and contributor(s) and not of MDPI and/or the editor(s). MDPI and/or the editor(s) disclaim responsibility for any injury to people or property resulting from any ideas, methods, instructions or products referred to in the content.